HIV-1 Viral Protein R Couples Metabolic Inflexibility With White Adipose Tissue Thermogenesis

Neeti Agarwal,[1] Dinakar Iyer,[2] Pradip Saha,[1] Aaron R. Cox,[1] Yan Xia,[3] Netanya S. Utay,[4] Anoma Somasundaram,[4] Ulrich Schubert,[5] Jordan E. Lake,[4] Sean M. Hartig,[1,3] and Ashok Balasubramanyam[1]

Diabetes 2021;70:2014–2025 | https://doi.org/10.2337/db20-0888

Persons living with HIV (PLWH) manifest chronic disorders of brown and white adipose tissues that lead to diabetes and metabolic syndrome. The mechanisms that link viral factors to defective adipose tissue function and abnormal energy balance in PLWH remain incompletely understood. Here, we explored how the HIV accessory protein viral protein R (Vpr) contributes to adaptive thermogenesis in two mouse models and human adipose tissues. Uncoupling protein 1 (UCP1) gene expression was strongly increased in subcutaneous white adipose tissue (WAT) biopsy specimens from PLWH and in subcutaneous WAT of the Vpr mice, with nearly equivalent mRNA copy number. Histology and functional studies confirmed beige transformation in subcutaneous but not visceral WAT in the Vpr mice. Measurements of energy balance indicated Vpr mice displayed metabolic inflexibility and could not shift efficiently from carbohydrate to fat metabolism during day-night cycles. Furthermore, Vpr mice showed a marked inability to defend body temperature when exposed to 4°C. Importantly, Vpr couples higher tissue catecholamine levels with UCP1 expression independent of β-adrenergic receptors. Our data reveal surprising deficits of adaptive thermogenesis that drive metabolic inefficiency in HIV-1 Vpr mouse models, providing an expanded role for viral factors in the pathogenesis of metabolic disorders in PLWH.

HIV and antiretroviral therapy (ART) are associated with adipose tissue (AT) dysfunction and systemic metabolic alterations (1), the cardinal features of which are intra-abdominal fat accumulation, fatty liver disease, dyslipidemia, insulin resistance, and diabetes. Viral factors enable the complex pathophysiology of these defects in persons living with HIV (PLWH) (2–4), but the mechanisms that link them to defective AT are not well understood. A paradoxical feature of metabolic dysregulation described in PLWH is the presence of adipocytes positive for uncoupling protein 1 (UCP1) in white AT (WAT) depots (5–9). In numerous experimental models, UCP1-postive adipocytes in WAT are associated with greater insulin sensitivity and more efficient energy metabolism (10). However, in PLWH, *UCP1* expression in WAT correlates with systemic defects in lipid and carbohydrate metabolism (7,11).

We previously established that the HIV accessory protein viral protein R (Vpr) circulates in the blood of PLWH even during "suppressive" ART (12,13) and causes hyperlipidemia, glucose intolerance, and dysregulated AT function in mice (12,13). In the current study, we identified UCP1-positive ("beige") adipocytes in subcutaneous WAT of Vpr mice and dissected the causes, thermogenic changes, and metabolic consequences of this phenomenon. We discovered that beige adipocytes in Vpr mice do not exert metabolic benefits, but mirror the complex disruption of the energy balance of PLWH on ART.

RESEARCH DESIGN AND METHODS

Study Design

We used two Vpr mouse models described previously (12,13). For gene and protein expression experiments,

[1]Division of Diabetes, Endocrinology, and Metabolism, Baylor College of Medicine, Houston, TX
[2]Department of Biology and Biochemistry, University of Houston, Houston, TX
[3]Department of Molecular and Cellular Biology, Baylor College of Medicine, Houston, TX
[4]Division of Infectious Diseases, Department of Internal Medicine, McGovern Medical School at the University of Texas Health Science Center, Houston, TX
[5]University of Erlangen, Erlangen, Germany

Corresponding author: Ashok Balasubramanyam, ashokb@bcm.edu

Received 1 September 2020 and accepted 29 June 2021

This article contains supplementary material online at https://doi.org/10.2337/figshare.14888103

groups of four to seven mice were compared with similar numbers of control mice. Sample sizes were based on our previous data regarding the effects of Vpr on AT (12,13). Male 14-week-old mice were used in most experiments.

Vpr-Transgenic Mice

FVBN mice expressing PEPCK promoter-driven Vpr under control of a tetracycline-repressible (tTA) system were constructed at the National Institutes of Health (NIH) (14).

Synthetic Vpr

Synthetic Vpr (sVpr) was produced by solid-state peptide synthesis, purified, characterized by sequencing and mass spectrometry, and compared with viral Vpr by SDS-PAGE and immunoblotting (15). Stability of the peptide in aqueous solution was confirmed by dynamic light scattering, circular dichroism and ^{1}H-nuclear magnetic resonance spectroscopy (15). Continuous delivery of sVpr or vehicle was achieved using ALZET pumps (model 1002; DURECT, Cupertino, CA) containing an aqueous solution of sVpr or sterile water. These were implanted subcutaneously in wild-type (WT) mice with a delivery rate of 0.25 μL/h to administer 5 μg of sVpr/24 h for 14 days (12–14).

Human Biopsy Samples

We measured UCP1 expression in subcutaneous AT biopsy specimens obtained from 9 PLWH on suppressive ART (16) and 10 control subjects without HIV to assess gene expression of markers of brown AT (BAT). For the PLWH, subcutaneous, lower abdominal AT samples were obtained by excisional biopsy from participants in the AIDS Clinical Trials Group protocol A5317 (16). The participants were 91% male, 82% non-White, aged 45 ± 11 years (mean ± SD), with BMI 25.9 ± 3.94 kg/m^2. Samples were preserved in RNAlater immediately after extraction and stored at −80°C until processing. Total RNA was isolated using the Aurum Total RNA Fatty and Fibrous Tissue kit (Bio-Rad Laboratories, Hercules, CA), and the concentration of the eluted RNA was measured and its quality confirmed using NanoDrop. Optical density 260-to-280 ratio values were ∼1.9. The control subjects were obese women with BMI of 38.3 ± 0.26 kg/m^2, HbA_{1c} of 4.59 ± 0.09%, aged 38.9 ± 10.9 years, of White European background, and taking no glucose- or lipid-lowering medications. WAT cDNA from these participants was derived from RNA obtained through abdominal subcutaneous biopsy specimens (17). RNA quality was measured using a Bioanalyzer (Agilent, Santa Clara, CA), and the RNA Integrity Number for the samples ranged between 5.8 and 9.7.

mRNA Levels

Total RNA was extracted from fat depots using the RNeasy Lipid Tissue Mini Kit (QIAGEN, Valencia, CA), transcribed using the RNA-to-cDNA kit (Applied Biosystems, Grand Island, NY), and PCR was performed using the TaqMan probe-based assay and Universal PCR Master Mix with a ABI 7000 Real-Time PCR System (Applied Biosystems). mRNA expression levels of the BAT marker genes uncoupling protein 1 (*Ucp1*), pyruvate dehydrogenase kinase-4 (*Pdk4*), prostaglandin-endoperoxide synthase-2 (*Ptgs2*), and iodothyronine deiodinase-2 (*Dio2*) were measured. *Pgk1* mRNA was used for normalization.

Ucp1 Quantification by Quantitative PCR

Quantitative (q)PCR was used to quantify *Ucp1* copy number in AT from humans and Vpr mice. The standards were human UCP1 (*hUcp1*) and mouse Ucp1 (*mUcp1*) genes cloned in a plasmid vector by the Baylor College of Medicine (BCM) Gene Vector Core and purified by minipreps. RNA from mouse AT depots was extracted and its quality confirmed by NanoDrop. qPCR was performed using SYBR Green Master Mix from Bio-Rad. Standards were serially diluted to ensure unknown samples fell in the linear portion of the standard curve. DNA copy number was calculated by converting base pairs of plasmid UCP1 DNAs to ng/mol, determining their mass using Avogadro's number, and deriving the titers (gene copy number/μL) from the dilution factor in the qPCR reaction.

Immunoblotting

Total protein was extracted from mouse fat depots using radioimmunoprecipitation assay buffer containing phosphatase and protease inhibitors. Protein was quantified using the Bradford reagent, resolved by SDS-PAGE, transferred to nitrocellulose membranes (Millipore, Billerica, MA), blocked with 5% milk/Tris-buffered saline with Tween, and detected using specific primary antibodies (1:1,000) with horseradish peroxidase-conjugated secondary antibodies (1:10,000) identified by enhanced chemiluminescence (Thermo Fisher, Grand Island, NY). Multiple replicate blots were prepared for each experiment, each with 50 μg total protein loaded per lane, and each probed with a different antibody. Primary antibodies were adipocyte triglyceride lipase (ATGL), HSP90, hormone-sensitive lipase, phosphorylated hormone-sensitive lipase at serine residue 563 (Cell Signaling, Danvers, MA), UCP1 (Abcam, Cambridge, MA), and β-actin (Sigma-Aldrich, St. Louis, MO). Immunoblotting of mitochondrial electron transport chain complexes was performed on whole-cell extracts from the total AT using MitoProfile Total OXPHOS Rodent WB Antibody Cocktail (ab110413, Abcam).

Histology

AT depots were removed, fixed with 4% paraformaldehyde in PBS for 24 h at 4°C, embedded in paraffin, and cut at 4-μm thickness. Sections were stained with hematoxylin-eosin, and immunostained using antibodies to UCP1 from Abcam. The BCM Human Tissue and Pathology Core performed sectioning, immunohistochemistry, and staining. Pictures of different fields were taken at

10× to 20× magnification (n = 3 mice per group) using a Keyence microscope (Keyence Corp., Itasca, IL).

Energy Balance Study

We used a 10-chamber Comprehensive Laboratory Animal Monitoring System-Home Cage (CLAMS-HC) system (Columbus Instruments, Columbus, OH) in the BCM Mouse Metabolism and Phenotyping Core. We performed three sets of experiments using Vpr-transgenic (Tg) and WT mice: *1*) quotidian: room temperature (RT) (21°C) for 24 h; *2*) short-term: cold temperature (4°C) for 6 h; or *3*) prolonged: 4°C for 6 h daily for 14 days. The prolonged cold exposure data set was analyzed using CalR software (18). Briefly, the raw data file from CLAMS-HC recordings were loaded into CalR, which performs automated analysis of indirect calorimetry data using mass variables as covariates.

Stromal Vascular Cell Preparation

AT depots were excised from Vpr-Tg, WT, sVpr-treated, vehicle-treated, and β-adrenergic receptor–less (β-less) mice (19). Stromal vascular fractions (SVF) were prepared from the AT depots. Briefly, tissues were minced and digested with collagenase, and then the cell suspensions were centrifuged to separate SVF cells from adipocytes. Separated SVF cells were treated with red blood cell lysis buffer, followed by washing with PBS. Cells were counted and plated in a 6-well plate or XF24 cell culture microplates from Agilent.

Differentiation of SVF Cells and Brown Preadipocytes

Plated SVF cells were placed in a cell culture incubator at 37°C and monitored daily. Two days after formation of a confluent monolayer, differentiation media (Zen-Bio, Research Triangle, NC) was added. After 48 h, the cells were transferred to adipocyte maintenance media (Zen-Bio). Maintenance media was changed every other day with care to avoid bursting lipid droplets. Brown preadipocytes (FVB-C3) were provided by Miao-Hsueh Chen (BCM) and cultured as previously described (20).

Seahorse Experiments

Respiration was determined with SVF-derived adipocytes using an XF24 analyzer (Seahorse Bioscience). Equal numbers of SVF preadipocytes were plated into V7-PS plates and allowed to grow to confluence before differentiation. Respiration analysis was performed using the Seahorse XF Cell Mito Stress Test Kit from Agilent according to the manufacturer's protocol. Before the experiment, the maintenance media was replaced by XF-DMEM supplemented with glucose (10 mmol/L), pyruvate (1 mmol/L), and glutamine (2 mmol/L). Ports were injected with the following drugs: 2 μmol/L oligomycin, 2 μmol/L carbonyl cyanide-4 (trifluoromethoxy) phenylhydrazone (FCCP), and 0.5 μmol/L rotenone/antimycin.

ELISA

Catecholamine concentrations in serum and AT were measured by ELISA (BioVision, Milpitas, CA) following the manufacturer's protocols.

Lentiviral Infection

Vpr cDNA was cloned into tetracycline-inducible lentivirus system constructs as described earlier (13). Viruses were packaged and propagated following a standard protocol in 293T cells (13,21,22). Virus particles were concentrated by ultracentrifugation and titered using Retro-X Kits (Clontech, Mountain View, CA). SVF prepared from WT or β-less mice were transduced with lentivirus constructs (TRE-rtTA or TRE-Vpr and rtTA) at 70% confluence. Adipocyte differentiation medium (Zen-Bio) was added 48 h later (day 2), followed by adipocyte maintenance medium (Zen-Bio). Vpr expression was induced by adding 1 μg/mL doxycycline to the cells on the 5th day after addition of the adipocyte differentiation cocktail. Cells were collected on day 10 for extraction of RNA and protein.

Mitochondrial DNA Quantification

Mitochondrial DNA content was determined by qPCR. Total DNA was isolated using the DNeasy kit (QIAGEN). Real-time PCR was performed on ABI 7000 Real-Time PCR System (Applied Biosystems) using SYBR Green qPCR SuperMix-UDG (Life Technologies). Reactions were prepared according to the manufacturer's recommendations in a total volume of 20 μL. mtDNA primers were designed using the mitochondrial genome sequence within the NADH dehydrogenase subunit-2 (*ND2*) gene. *18S* rRNA was used as the invariant control.

Statistics

All experiments involved two-way ANOVA comparisons between Vpr and WT groups. Two-tailed, unpaired t tests for unequal variance were used. $P < 0.05$ was considered significant.

Study Approval

The BCM Institutional Animal Care and Use Committee approved all animal protocols. All animals received humane care according to criteria in the *Guide for the Care and Use of Laboratory Animals* (NIH publication 86-23, revised 1985).

Written informed consent was obtained from all human participants prior to inclusion in the study. For the PLWH, the AT biopsy samples were obtained as part of a network study (AIDS Clinical Trials Group protocol A5317). All sites in the network received local institutional review board approval, and the NIH Division of AIDS reviewed the approvals before allowing each site to open the study (NCT01928927). For the human control subjects, the AT biopsy studies were approved by the Karolinska Institutet Ethics Committee (Dnr 2008/2.3) and the BCM Institutional Review Board (H-28439).

Data and Resource Availability

Data and resources for the work presented here will be available from the corresponding author upon reasonable request.

RESULTS

PLWH and Vpr Mice Express UCP1 at Elevated Levels in Subcutaneous WAT

Reports of UCP1-positive adipocytes in subcutaneous WAT of PLWH led us to assess the levels of UCP1, the defining marker of thermogenesis, in subcutaneous AT of PLWH and Vpr mice. PLWH on suppressive (HIV-1 RNA <50 copies/mL) ART had markedly higher *UCP1* mRNA levels in abdominal subcutaneous AT biopsy specimens relative to control subjects without HIV (Fig. 1*A*). Similarly, sVpr-treated mice also had higher *Ucp1* mRNA copy numbers compared with vehicle-treated mice in inguinal (subcutaneous) WAT (Fig. 1*B*). Vpr-Tg mice also showed higher *Ucp1* mRNA copy numbers in inguinal WAT (iWAT) depots compared with WT littermates (Fig. 1*C*). Copy number analysis indicated the elevated *Ucp1* levels in sVpr mice were similar to those of PLWH. Subcutaneous WAT from PLWH and HIV mouse models consistently showed two- to sixfold higher *Ucp1* mRNA levels than matched control subjects.

Subcutaneous WAT From Vpr Mice at RT Shows Evidence of White-to-Beige Adipocyte Conversion

To understand whether *Ucp1* copy number in iWAT reflected characteristics of BAT, we explored thermogenic gene expression and morphology of iWAT in Vpr mice. *Ucp1* mRNA expression was upregulated in iWAT of Vpr-Tg mice compared with WT littermates (Fig. 2*A*) and in iWAT of sVpr-treated compared with vehicle-treated mice (Fig. 2*B*). The mRNA expression of *Pdk4* was upregulated and that of *Dio2*, another key marker of BAT, trended higher (P = 0.08) in sVpr-treated compared with vehicle-treated mice (Fig. 2*B*). Changes in brown adipocyte marker genes were specific to iWAT because mRNA levels of *Ucp1* and *Dio2* in BAT were similar between both Vpr mouse models and their respective controls (Fig. 2*C* and *D*). UCP1 protein was also increased in both iWAT of Vpr-Tg versus WT mice (Fig. 2*E*) and in sVpr-treated versus vehicle-treated mice (Fig. 2*F*). UCP1 protein levels were variable but overall not different in BAT of Vpr-Tg versus WT littermates (Fig. 2*E*) and in sVpr-treated versus vehicle-treated mice (Fig. 2*F*).

Histological examination iWAT of Vpr-Tg and sVpr-treated mice showed morphological changes similar to classical BAT that were not observed in their respective controls, including UCP1-positive adipocytes that were smaller in size and contained multilocular lipid droplets (Fig. 2*G* and Supplementary Fig. 1*A*). Immunohistochemistry demonstrated increased UCP1 protein expression in the iWAT of Vpr-Tg and sVpr-treated mice compared with their controls, without impacting UCP1 expression in BAT (Fig. 2*H* and Supplementary Fig. 1*B*). These data indicate Vpr induces white-to-beige adipocyte conversion in iWAT with elevated expression of thermogenic markers.

Energy Balance and Physical Activity Are Altered in Vpr Mice at RT

Transformation of WAT to BAT-like (beige) fat often coincides with increased VO_2 and thermogenesis. To investigate these changes in the Vpr mice, we performed extensive energy balance and physical activity measurements in the CLAMS-HC metabolic cages. Over 24-h observation at RT, Vpr-Tg mice showed decreased VO_2 (117.10 ± 2.73 vs. 133.63 ± 3.41 mL/h; P = 0.01) (Fig. 3*A*) and VCO_2 (99.26 ± 2.22 vs. 111.16 ± 2.61 mL/h; P = 0.01) (Fig. 3*B*). VO_2 and VCO_2 were decreased in the Vpr-Tg mice during both light and dark phases of the day (VO_2: 119.87 ± 3.47 vs. 133.41 ± 4.10 mL/h in the light phase, P = 0.05; 109.32 ± 2.2 vs. 129.39 ± 3.77 mL/h in the dark phase, P = 0.005; VCO_2: 98.63 ± 2.44 vs. 108.25 ± 3.45 mL/h in the light phase, P = 0.07; 94.14 ±

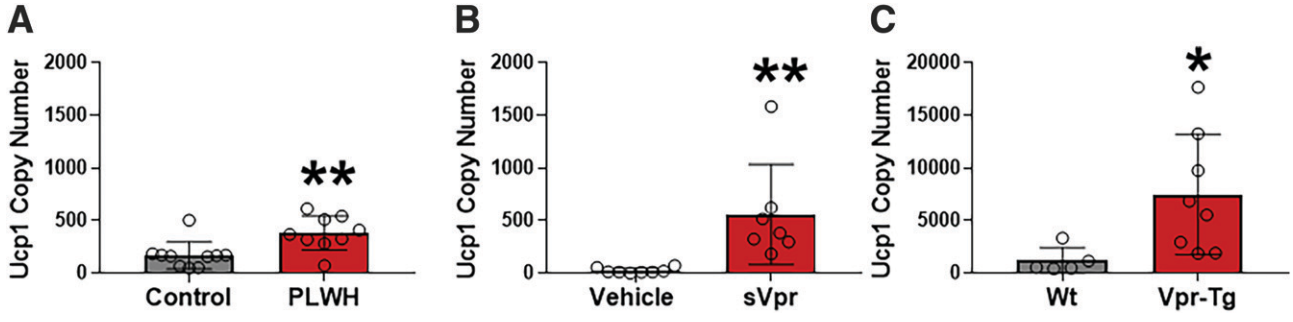

Figure 1—UCP1 mRNA copy number is elevated in subcutaneous WAT of PLWH and Vpr mice. *A*: *UCP1* copy number in abdominal subcutaneous WAT of PLWH (n = 9) compared with healthy human control subjects (n = 10). *Ucp1* copy number in inguinal WAT of sVpr-treated (n = 7) compared with vehicle-treated (n = 8) mice (*B*) and in inguinal WAT Vpr-Tg (n = 8) compared with WT littermates (n = 5) (*C*). Values are mean ± SD. Two-tailed, unpaired t tests for unequal variance were used. $P < 0.05$ was considered significant. *$P < 0.05$, **$P < 0.01$.

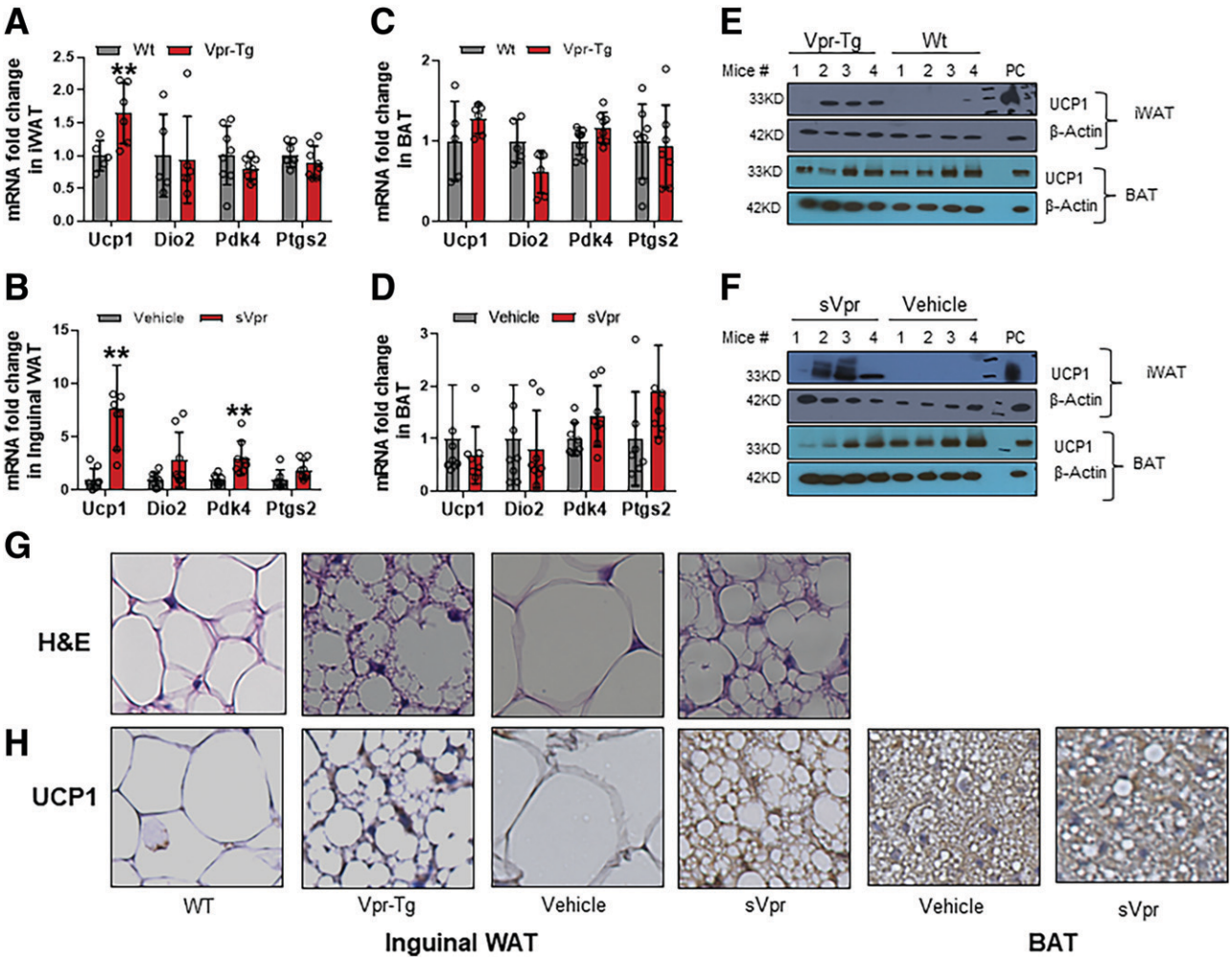

Figure 2—Vpr induces conversion of subcutaneous WAT to BAT-like phenotype. *Ucp1* mRNA is increased in inguinal WAT of Vpr-Tg (n = 6–8) compared with WT (n = 5–8) mice (*A*) and in sVpr-treated (n = 7–8) compared with vehicle-treated (n = 7–8) mice (*B*). *Ucp1* expression is similar in BAT of Vpr-Tg (n = 6–8) compared with WT (n = 5–8) mice (*C*) and in sVpr-treated (n = 7–8) compared with vehicle-treated (n = 7–8) mice (*D*). Protein expression of UCP1 is increased in iWAT of Vpr-Tg compared with WT mice (*E*) and in sVpr-treated compared with vehicle-treated mice (*F*). *G*: Hematoxylin-eosin (H&E) stain shows transformation to a BAT phenotype in iWAT of Vpr-Tg compared with WT mice and in sVpr-treated compared with vehicle-treated mice. *H*: UCP1 expression (immunohistochemistry) is increased in iWAT of Vpr-Tg compared with WT mice and sVpr-treated compared with vehicle-treated mice, and in BAT of sVpr-treated compared with vehicle-treated mice. Images were cropped at similar magnification. PC, positive control BAT. Two-tailed, unpaired t tests for unequal variance were used. $P < 0.05$ was considered significant. Values are mean ± SD. $^{**}P < 0.01$.

2.08 vs. 108.71 ± 3.54 mL/h in the dark phase, P = 0.01) (Fig. 3*E* and *F*). The overall respiratory exchange ratio (RER) was not different in Vpr-Tg compared with WT mice (0.85 ± 0.01 vs. 0.83 ± 0.01; P = 0.325) (Fig. 3*C*). However, the Vpr-Tg mice had increased RER in the dark phase compared with the light phase (0.87 ± 0.01 vs. 0.82 ± 0.004; P = 0.001) (Fig. 3*G*) and showed a trend toward elevated RER compared with WT mice (indicating diminished selection of fat for oxidation) in the dark phase (0.87 ± 0.004 vs. 0.84 ± 0.004; P = 0.08) (Fig. 3*G*). The altered energy balance was not explained by physical activity changes when the entire 24-h period was considered (1,277 ± 170 vs. 1,041 ± 150 activity counts; P = 0.4) (Fig. 3*D*). However, during the light phase, the Vpr-Tg mice were more active than the WT mice (1,942 ± 239 vs. 935 ± 88 activity counts, P = 0.04), with a nonsignificant decrease in activity during the dark phase (Fig. 3*H*). The Vpr-Tg mice showed a trend toward increased food intake during the dark phase compared with the WT mice (2.62 ± 0.36 vs. 1.56 ± 0.31 g; P = 0.08), with no difference during the light phase (Fig. 3*I*). Finally, at RT, Vpr-Tg mice showed no differences compared with WT mice in body weight (34 ± 0.88 vs. 33 ± 0.80 g; P = 0.5) or body temperature (37.10 ± 0.58 vs. 38.14 ± 0.17°C; P = 0.2) over the 24-h period (Fig. 3*J* and *K*).

Vpr Mice Are Unable to Defend Body Temperature After Short-term Exposure to 4°C

Thermogenic activity in beige and brown AT increases after exposure to cold conditions. Hence, we measured

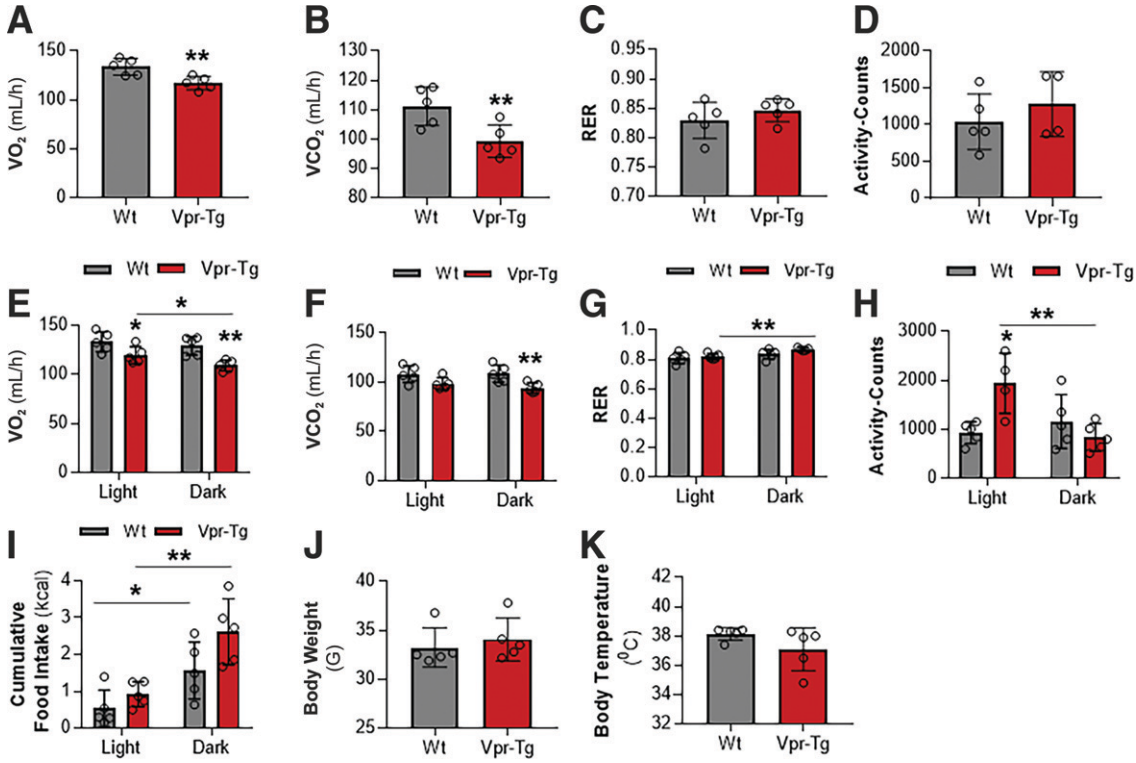

Figure 3—Energy balance and physical activity are altered in Vpr-Tg mice at RT. Vpr-Tg mice manifest decreased VO_2 (*A*) and VCO_2 (*B*) compared with WT mice over 24 h. RER (*C*) and activity (*D*) are not different in the two groups of mice. Vpr-Tg mice manifest decreased VO_2 (*E*) and VCO_2 (*F*) during both light and dark phases compared with WT mice. Increased RER in the Vpr-Tg mice occurs predominantly in the dark phase (*G*); conversely, Vpr-Tg mice are more active compared with WT mice in the light phase but not in the dark phase (*H*). *I*: Vpr-Tg mice display increased feeding behavior in the dark phase compared with WT mice. Body weight (*J*) and body temperature (*K*) do not differ between the two groups of mice at the end of the 24-h cycle. Values are mean ± SD. Two-tailed, unpaired *t* tests for unequal variance were used. $P < 0.05$ was considered significant. *$P < 0.05$; **$P < 0.01$; $n = 5$ in each group.

energy balance, physical activity, and feeding behavior in the mice during short-term exposure to cold temperature. Measurements were recorded every 15–20 min during 6 h of exposure to 4°C, and the average values were calculated. Vpr-Tg mice showed a trend toward lower VO_2 (144.70 ± 14.16 vs. 181.94 ± 3.71 mL/h; $P = 0.07$) (Fig. 4*A*) and VCO_2 (115.28 ± 11.24 vs. 146.08 ± 3.87 mL/h; $P = 0.06$) (Fig. 4*B*) compared with WT littermates when exposed to 4°C for 6 h in the CLAMS-HC chambers. RER (0.80 ± 0.01 vs. 0.80 ± 0.01, $P = 0.8$) (Fig. 4*C*) and activity (851 ± 134 vs. 762 ± 61 activity counts, $P = 0.6$ (Fig. 4*D*) were not different in the two groups under these conditions. Body weights also were not different between the two groups, before (34 ± 0.88 vs. 33 ± 80 g, $P = 0.5$) or after cold exposure (33 ± 0.66 vs. 32 ± 0.65 g, $P = 0.2$) (Fig. 4*E*). However, Vpr-Tg mice had significantly lower core body temperature than WT mice after cold exposure (32.42 ± 0.35 vs. 36.24 ± 0.25°C, $P < 0.0001$ (Fig. 4*F*), with the difference becoming apparent 2 h into the cold exposure period and continuing to decline at 6 h without stabilizing (Fig. 4G). There were also significant increases in the plasma levels of free fatty acids (0.95 ± 0.02 vs. 0.86 ± 0.02 mEq/L, $P = 0.03$) (Fig. 4*H*), triglycerides (61 ± 6.5 vs. 38 ± 4.5 mg/dL, $P = 0.009$) (Fig. 4*I*), and total cholesterol (220 ± 16 vs. 167 ± 5 mg/dL, $P = 0.02$) (Fig. 4*J*) concentrations in Vpr-Tg compared with WT mice after 6 h of cold exposure.

Vpr Mice Do Not Defend Body Temperature and Display Impaired Energy Balance During Prolonged Cold Exposure

To understand long-term thermogenic defects resulting from Vpr expression, mice were repeatedly exposed to 4°C (6 h daily) over 14 days, using the protocol shown schematically in Fig. 5*A*. Vpr-Tg mice showed lower VO_2 (173 ± 1.9 vs. 204 ± 1.4 mL/h; $P = 0.005$) (Fig. 5*B*) and VCO_2 (153 ± 2.6 vs. 174 ± 1.2 mL/h; $P = 0.04$) (Fig. 5*C*). VO_2 was lower in the Vpr-Tg mice during both cold and RT periods (244 ± 0.65 vs. 279 ± 1.8 mL/h in the cold period, $P = 0.001$; 151 ± 1.92 vs. 174 ± 3 mL/h in the RT period, $P = 0.008$) (Fig. 5*B*); and VCO_2 was lower in the cold period (198 ± 1.2 vs. 224 ± 0.79 mL/h, $P = 0.004$) (Fig. 5*C*) but not in the RT period (139 ± 4.6 vs. 149 ± 5.4 mL/h, $P = 0.25$) (Fig. 5*C*). Vpr-Tg mice expended less energy than WT mice (0.85 ± 0.01 vs. 0.99 ± 0.007 kcal/h; $P = 0.01$) (Fig. 5*D*), and this occurred during both cold and RT periods (1.18 ± 0.004 vs. 1.34 ± 0.006 kcal/h in the cold period, $P = 0.0003$; 0.72 ± 0.01 vs. 0.83 ± 0.02 kcal/h in the RT

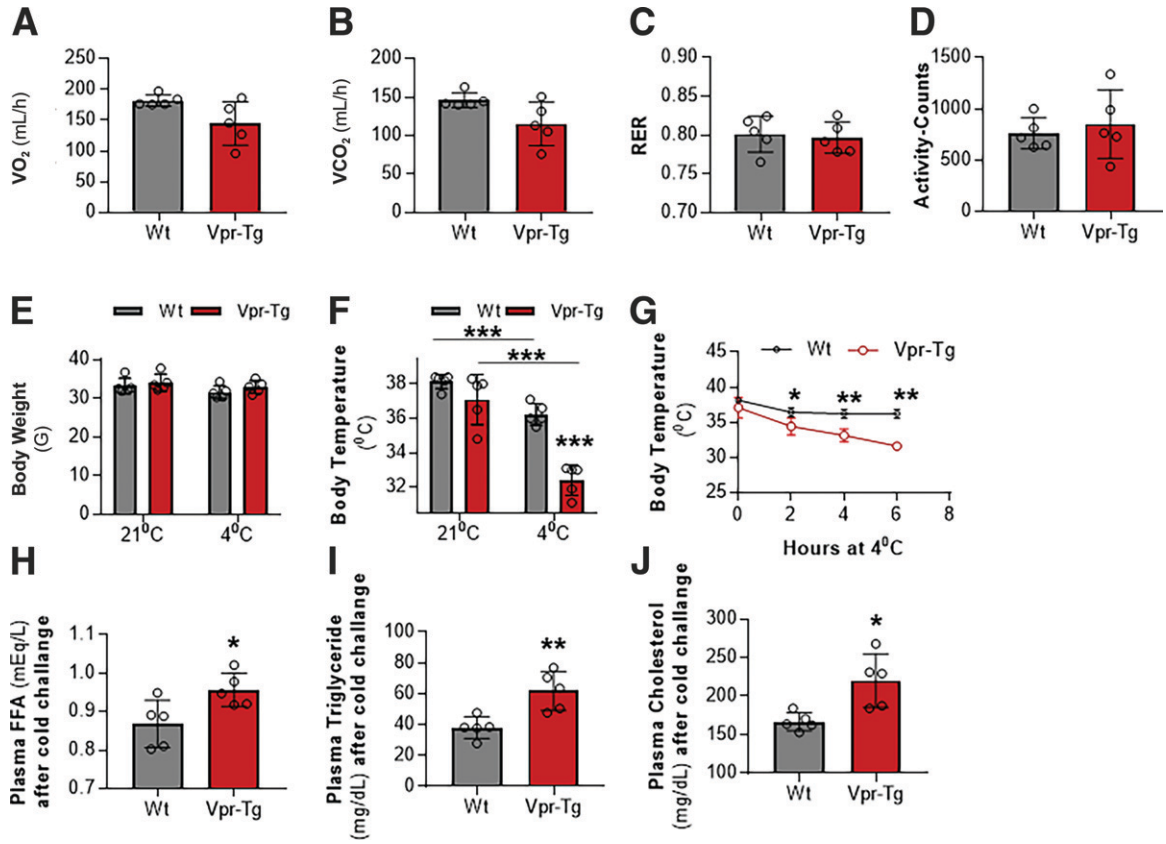

Figure 4—Vpr-Tg mice fail to defend body temperature upon short-term cold exposure. After exposure to 4°C for 6 h, Vpr-Tg mice trend toward decreased VO_2 (*A*) and VCO_2 (*B*) compared with WT mice, but RER (*C*) and activity levels (*D*) are not different between the two groups. *E*: Body weights of the two groups of mice are similar after 6 h of cold exposure. Core body temperature declines significantly more (*F*) and continuously (*G*) in Vpr-Tg mice compared with WT mice over the 6 h of cold exposure. Plasma free fatty acid (FFA) (*H*), triglycerides (*I*), and total cholesterol (*J*) levels are elevated in Vpr-Tg mice compared with WT mice after 6 h of cold exposure. Values are mean ± SD. Two-tailed, unpaired *t* tests for unequal variance were used. $P < 0.05$ was considered significant. *$P < 0.05$; **$P < 0.01$; ***$P < 0.001$; $n = 5$ in each group.

period, $P = 0.03$) (Fig. 5*D*). RER over 24 h was not different in the two groups (0.89 ± 0.02 vs. 0.86 ± 0.002; $P = 0.28$) (Fig. 5*E*). However, RER was increased in Vpr-Tg mice during the cold period (0.82 ± 0.004 vs. 0.79 ± 0.006; $P = 0.04$) (Fig. 5*E*), with no difference in the RT period (0.93 ± 0.01 vs. 0.88 ± 0.005; $P = 0.15$) (Fig. 5*E*).

The Vpr-Tg mice appeared to consume more food than WT mice over 24 h and during both periods, but the group difference did not achieve statistical significance due to interanimal variability (491 ± 127 vs. 108 ± 8 g over 24 h, $P = 0.2$) (Fig. 5*F*). Initial body weights before cold exposure were not different between the two groups (29 ± 1 vs. 31 ± 1.33 g, $P = 0.4$), but the Vpr-Tg mice weighed less than WT mice at the end of the 14 days of repeated cold exposure (20 ± 0.10 vs. 28 ± 0.92 g, $P = 0.02$) (Fig. 5*G*). Weight loss was significantly greater ($P = 0.04$) in the Vpr-Tg mice (~30%) compared with the WT mice (~10%) (Fig. 5*H*). AT mass was markedly reduced in Vpr-Tg compared with WT mice in all depots: iWAT (0.07 ± 0.009 vs. 0.72 ± 0.20% body weight, $P = 0.02$), perigonadal fat (0 ± 0 vs. 1.01 ± 0.14% body weight, $P = 0.001$), and BAT (0.08 ± 0.01 vs. 0.17 ± 0.01% body weight, $P = 0.003$) (Fig. 5*I*).

Core body temperature of the Vpr-Tg mice was similar to that of WT mice at RT (37.25 ± 0.24 vs. 36.98 ± 0.30°C $P = 0.45$) (Fig. 5*J*). The Vpr-Tg mice displayed a constant decline in core body temperature over the 14 days, whereas the WT mice maintained their core temperature in a physiological manner during this period (mean temperature over 14 days, taken daily at the end of the 6 h exposure to 4°C: 32.52 ± 0.49 vs. 35.26 ± 0.0.42°C, $P = 0.004$) (Fig. 5*J*). The maximum decline in the Vpr-Tg mouse core temperature occurred after 2 days of cold exposure (34 ± 0.68 vs. 36.2 ± 0.34°C, $P = 0.03$), and their core temperature thereafter remained lower than that of the WT mice (Fig. 5*K*).

Vpr Mice Show Catecholamine Resistance in Beige Adipocytes

To determine whether Vpr expression functionally drives AT thermogenesis, we performed ex vivo cellular respiration measurements on cultured SVF-derived adipocytes

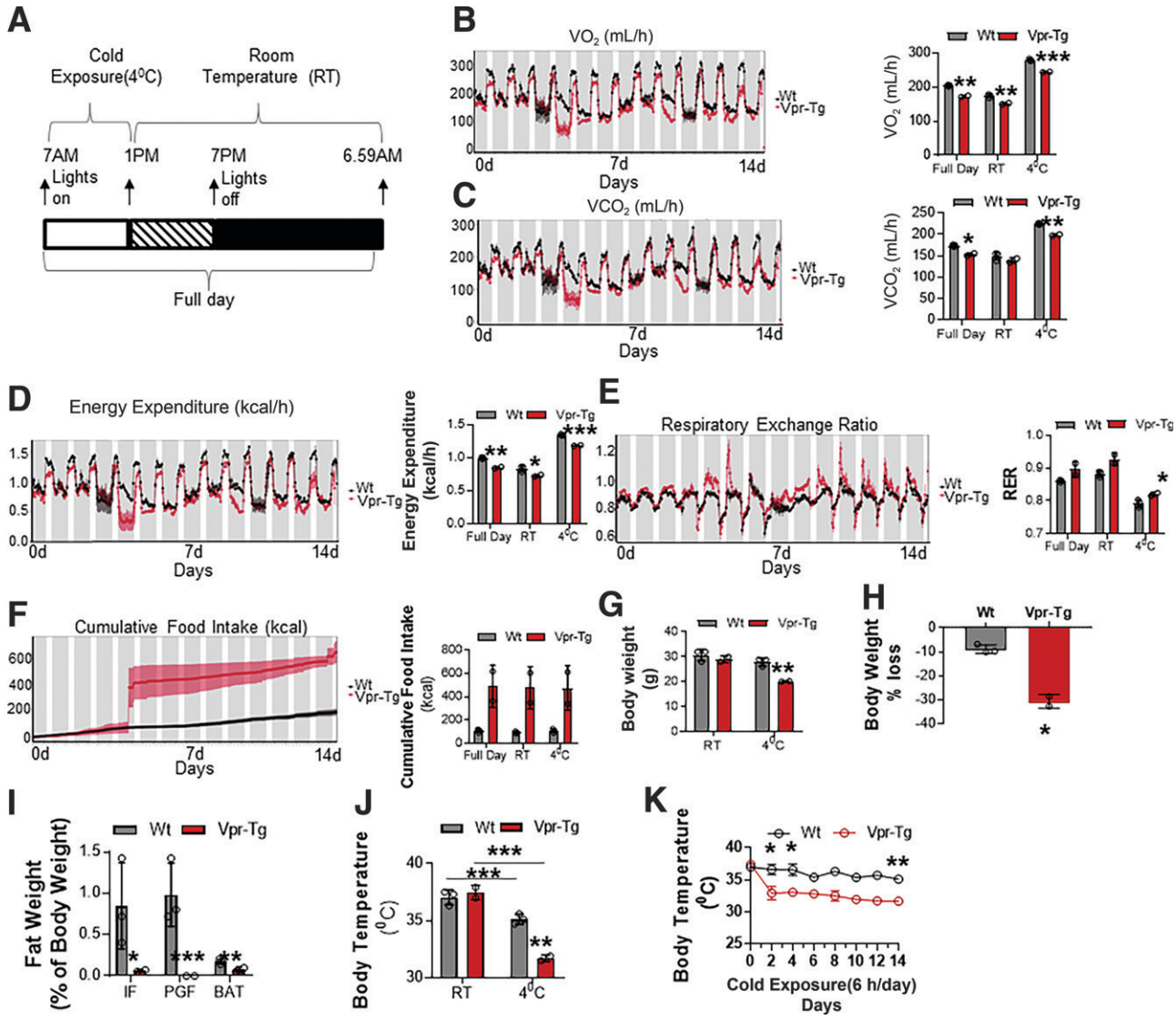

Figure 5—Vpr-Tg mice fail to defend body temperature upon prolonged cold exposure. *A*: Vpr-Tg and WT mice were exposed to 4°C for 6 h daily for 14 days, according to the protocol shown schematically. Vpr-Tg mice show decreased VO_2 (*B*), VCO_2 (*C*), and energy expenditure (*D*), with increased RER (*E*) and food consumption (*F*) compared with WT mice during prolonged cold exposure. *G*: Vpr-Tg mice display increased body weight compared with WT mice after prolonged cold exposure. *H*: Weight loss as the percentage of body mass change is greater in Vpr-Tg mice than in WT mice after prolonged cold exposure. *I*: Vpr-Tg mice have significantly lower fat mass than WT mice in all adipose tissue depots as the percentage of body weight after prolonged cold exposure. PGF, perigonadal fat. Although core body temperature declines after prolonged cold exposure in both Vpr-Tg and WT mice, it declines further (*J*) and more steeply and continuously in Vpr-Tg mice (*K*) over the 14-day period. Values are mean ± SD. Two-tailed, unpaired *t* tests for unequal variance were used. $P < 0.05$ was considered significant. *$P < 0.05$; **$P < 0.01$; ***$P < 0.001$; $n = 2$ Vpr-Tg and $n = 3$ WT mice in each group.

from WAT and BAT of the Vpr mouse models. We observed that adipocytes derived from iWAT of both Vpr mouse models undergo a white-to-brown transition reflected by augmented respiration (Fig. 6*A*). Cellular respiration was markedly and selectively increased in primary adipocytes derived from Vpr-Tg iWAT (subcutaneous), as measured by VO_2. Strikingly, this change did not occur in perigonadal (visceral) WAT adipocytes (Fig. 6*B*). SVF-derived BAT adipocytes from Vpr mice also showed higher VO_2 than those of WT mice (Fig. 6*C*). These results show that Vpr drives thermogenesis consistent with beige adipocyte transformation within iWAT in a cell-autonomous manner. To understand whether the increased oxygen consumption rate (OCR) in Vpr mice is due to increased mitochondrial mass, we measured mitochondrial *Nd2* (*mtND2*) expression and mitochondrial complex protein expression. *mtNd2* expression was not different in Vpr-Tg compared with WT mice (Fig. 6*D*) or sVpr-treated compared with vehicle-treated mice (Fig. 6*E*) in iWAT as well as perigonadal WAT. Amounts of mitochondrial complex

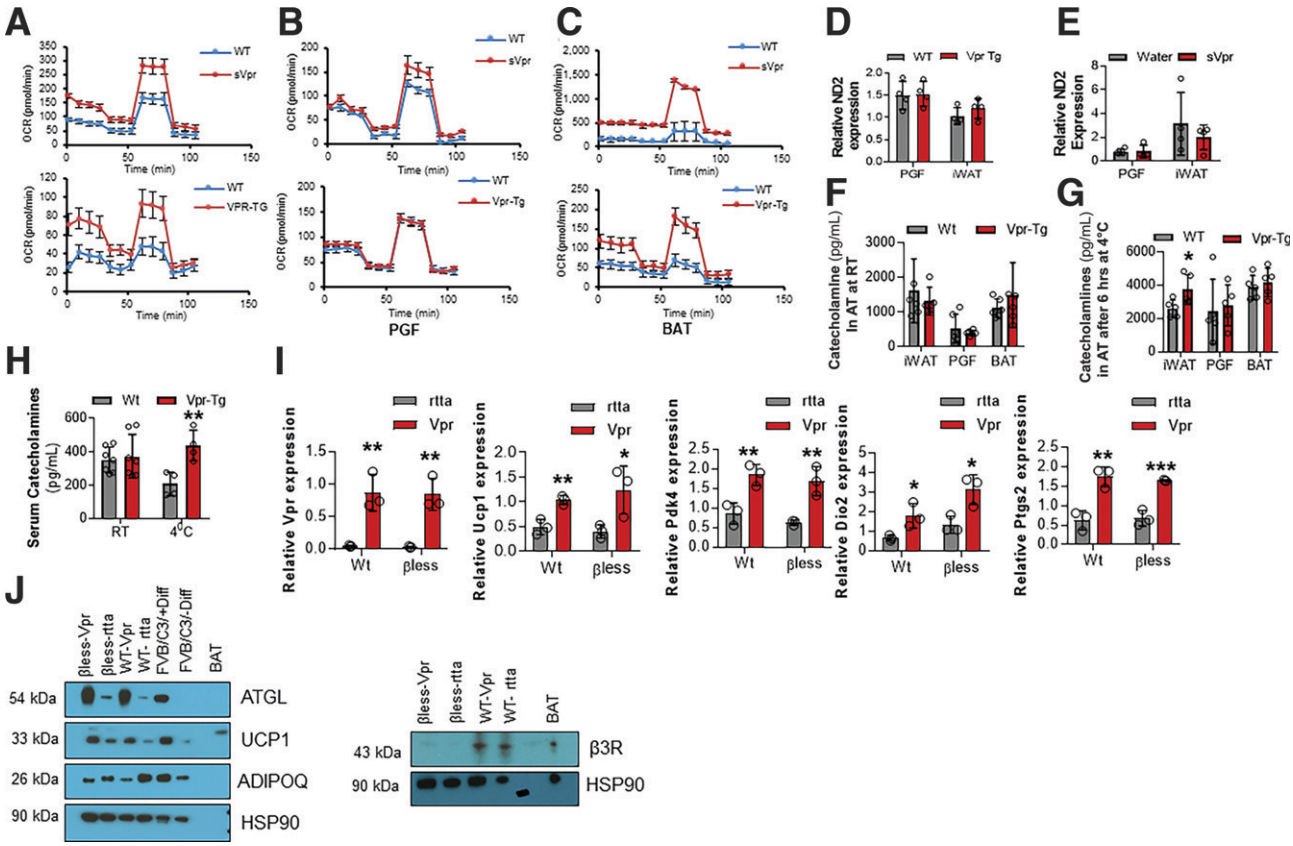

Figure 6—Thermogenesis is altered in adipocytes derived from inguinal (subcutaneous) WAT but not perigonadal (visceral) WAT or BAT of Vpr mice. *A*: Oxygen consumption rates (OCR) are increased in inguinal WAT adipocytes of sVpr-treated ($n = 4$) compared with vehicle-treated mice ($n = 4$) and of Vpr-Tg ($n = 6$) compared with WT mice ($n = 4$). *B*: OCR is similar in WAT adipocytes in perigonadal fat (PGF) of sVpr-treated ($n = 5$) compared with vehicle-treated ($n = 5$) mice, and of Vpr-Tg ($n = 5$) compared with WT ($n = 5$) mice. *C*: OCR is increased in BAT adipocytes of sVpr-treated ($n = 4$) compared with vehicle-treated ($n = 2$) mice, and of Vpr-Tg ($n = 3$) compared with WT ($n = 4$) mice. *mtNd2* expression is not different in Vpr-Tg ($n = 4$) compared with WT ($n = 4$) mice (*D*) and of sVpr-treated ($n = 4$) compared with vehicle-treated ($n = 4$) mice (*E*) in perigonadal WAT as well as inguinal WAT. *F*: Catecholamine content is similar in WAT and BAT depots of Vpr-Tg mice compared with WT mice at RT ($n = 5$–7). *G*: Catecholamine content is elevated in iWAT but not in perigonadal WAT or BAT of Vpr-Tg mice compared with WT mice after exposure to 4°C for 6 h ($n = 5$–7). *H*: Serum catecholamine levels are similar in Vpr-Tg compared with WT mice at RT; however, they are elevated in Vpr-Tg compared with WT mice after exposure to 4°C for 6 h ($n = 5$–7). *I*. qPCR of Vpr and beige fat marker genes in SVF-derived adipocytes that express Vpr or control (rtta) vectors ($n = 3$). *J*: Immunoblots show increased ATGL and UCP1 protein expression and decreased adiponectin protein expression in iWAT-derived mature adipocytes of WT and β-less mice, in which Vpr or control vector was expressed via lentiviral infection. β_3-receptor (β3R) was expressed in just WT cells and not β-less cells. PC, positive control BAT. FVB/C3, immortalized brown preadipocyte cell line was used as an additional positive control. Values are mean ± SD. Two-tailed, unpaired *t* tests for unequal variance were used. $P < 0.05$ was considered significant. *$P < 0.05$; **$P < 0.01$; ***$P < 0.001$.

proteins in all fat depots isolated from the Vpr mouse models were similar to those of the controls (Supplementary Fig. 2).

Cold exposure increases serum catecholamines to stimulate the mobilization of stored triglycerides in adipocytes and accommodate energy demands in other tissues. Catecholamine levels were not different within different AT depots of Vpr-Tg compared with WT mice at RT (Fig. 6*F*). However, after cold exposure for 6 h, catecholamine levels were significantly upregulated in iWAT of Vpr-Tg compared with WT mice (3,737 ± 402 vs. 2,607 ± 231 pg/mL, $P = 0.04$), but not in perigonadal WAT (2,788 ± 553 vs. 2,422 ± 869 pg/mL, $P = 0.7$) or BAT (4,180 ± 387 vs. 3,868 ± 324 pg/mL, $P = 0.5$) (Fig. 6*G*). Serum catecholamine concentrations were not different in Vpr-Tg compared with WT mice (374 ± 49 vs. 353 ± 29 pg/mL, $P = 0.7$) (Fig. 6*H*) at RT. After exposure to 4°C for 6 h, serum catecholamine levels were significantly elevated in Vpr-Tg compared with WT mice (401 ± 51 vs. 207 ± 36 pg/mL; $P = 0.01$) (Fig. 6*H*).

The cold-stimulated increase in the sympathetic drive to iWAT raised the question of whether the upregulation of UCP1 in that AT depot depends on β-adrenergic signaling. To this end, we investigated the effects of driving Vpr expression using an inducible lentiviral construct in

mature adipocytes derived from iWAT of WT mice or β-less mice, which lack all three β-adrenergic receptors (19). qPCR validated Vpr overexpression in mature adipocytes derived from iWAT of WT mice or β-less mice (Fig. 6*I*). *Ucp1* mRNA expression was upregulated in mature adipocytes derived from the subcutaneous fat of WT mice and β-less mice expressing Vpr compared with rtta (empty vector) (Fig. 6*I*). Similarly, we observed increased mRNA expression of other key markers related to the brown fat phenotype, including *Pdk4*, *Dio2*, and *Ptgs2* in WT cells and in β-less cells of mature adipocytes from subcutaneous fat expressing Vpr compared with control-treated differentiated adipocytes (Fig. 6*I*). As predicted, only WT cells showed β_3-adrenergic receptor expression but not β-less cells (Fig. 6*J*). Levels of UCP1 protein and that of the critical lipolytic enzyme ATGL were increased in both WT cells and β-less cells expressing Vpr compared with rtta (Fig. 6*J*). The increased levels of ATGL confirmed our previous finding in studies related to the upregulation of AT lipolysis by Vpr (13). Indeed, Vpr-induced UCP1 and ATGL levels were higher in the β-less cells than in the WT cells, suggesting Vpr supplants β-adrenergic signaling to upregulate the expression of these proteins. These changes were not observed with lentiviral expression of the control (rtta) vector in the respective cell types. In contrast, but consistent with our previous observations (13), Vpr expression reduced adiponectin (ADIPOQ) protein levels in a β-adrenergic receptor–dependent way (Fig. 6*J*).

DISCUSSION

Our findings demonstrate profound and unique HIV-1 Vpr-induced dysregulation of AT energy balance and thermogenesis, along with structural and functional changes in subcutaneous WAT that mirror those observed in PLWH (5–9). Subcutaneous WAT in PLWH and, selectively, iWAT of Vpr mice both demonstrate increased UCP1 expression to similar extents compared with controls, together with histological transformation of adipocytes in these depots to a "beige" phenotype. Whereas beiging of WAT usually improves metabolic efficiency and insulin sensitivity (23–31), in the Vpr mice it is associated with metabolic inefficiency and insulin resistance (12,13). A similar paradox occurs in PLWH (6–8,11). In treated HIV, viral persistence may drive these metabolic perturbations independent of ART effects.

We have shown AT is a reservoir for HIV (32–34), and Vpr causes differentiation defects in preadipocytes and excessive lipolysis in adipocytes (13). Adipocyte differentiation must engage lipogenesis and appropriately balance lipolysis to sustain responsiveness to insulin and maintain proper endocrine function. However, WAT from Vpr mice does not respond to insulin appropriately to restrain lipolysis and permit lipogenesis as needed to meet energy demands (13). Recent studies indicate lipogenesis supplies the fatty acid substrates required for UCP1-driven thermogenesis (35). Without this metabolic coupling, and in the setting of hyper-lipolytic Vpr-affected adipocytes (13), beige or brown AT do not perform thermogenesis physiologically despite direct upregulation of UCP1 expression by Vpr. This phenomenon is most clearly observed after cold exposure, when the Vpr mouse displays *1*) increased fatty acid and lipid release; *2*) inability to maintain core body temperature; and *3*) an almost complete depletion of AT stores.

The current data explain the mechanism underlying this paradox with regard to energy balance and thermogenesis. Recruitment of UCP1-positive cells in subcutaneous WAT increases VO_2 and energy expenditure in rodents (10). At RT, Vpr mice demonstrate decreased VO_2 compared with controls, despite increased physical activity during the light phase. When exposed to cold temperature, the Vpr mice increase VO_2 significantly less than the control mice, a defect associated with a marked inability to maintain core body temperature. The apparent discrepancy between high UCP1 but not elevated thermogenesis concurs with recent reports (36–38) that demonstrate the presence of UCP1 may not uniformly support elevated energy expenditure or exert therapeutic benefits (38).

Mammals engage an adaptive thermogenic response through coordinated central and sympathetic nervous system outflow to AT to generate heat from stored fatty acid substrates and maintain body temperature. To this end, AT nerve fibers supply catecholamines for activation of β-adrenergic receptors and consequent UCP1 induction for heat generation in beige adipocytes and BAT. Our models suggest that Vpr expression increases sympathetic tone and constitutively elevates lipolysis independent of β-adrenergic receptor activity. Subcutaneous WAT of Vpr mice shows unique and exclusive heightened *Ucp1* expression, but not of other canonical mRNA targets of browning, including *Dio2* and *Ptgs2*. This phenomenon likely reflects dissociated β-adrenergic receptor activity from other known stimuli of browning, including thyroid hormone (36).

Acute β-adrenergic receptor activity stimulates the interferon/Stat1 pathway and accumulates myeloid responses in subcutaneous WAT of rodents (38). Along these lines, hypermetabolic responses in PLWH and Vpr mouse models couple aberrant lipolysis with myeloid immune cell infiltration (13). Chronic inflammation in WAT, as occurs in PLWH (39–42), frequently causes insensitivity to catecholamines (39,43). Hence, we propose Vpr (and perhaps other factors released by HIV-1) provokes a confluence of chronic maladaptive thermogenesis and inflammatory responses in WAT (13) that results in dyslipidemia and insulin resistance in PLWH.

Our UCP1 data in PLWH differ somewhat from other studies (6,8). Srinivasa et al. (8) described decreased UCP1 expression in 18 subcutaneous abdominal punch biopsy specimens from PLWH being associated with longer ART duration, particularly use of integrase strand transfer

inhibitors (INSTIs), which are known to penetrate into AT (44). A potential explanation for the difference may be that whereas punch biopsy specimens procure superficial WAT, our samples obtained by surgical excision were composed of WAT from a deeper abdominal subcutaneous AT layer. Deep subcutaneous AT has been associated with greater metabolic and inflammatory activity than superficial subcutaneous AT (45). Our participants also differed from those studied by Srinivasa et al. (8) in mean age, sex distribution, and race/ethnicity. We do not have information on ART use and duration of HIV from the PLWH who provided our human samples. These differences preclude direct comparison between the two studies. Although our human control subjects were not matched for sex with our PLWH participants, it is notable that the predominately female control subjects would be expected to have higher UCP1 levels in subcutaneous AT than the predominantly male PLWH participants based on reported sex differences in WAT UCP1 expression (46,47), yet UCP1 levels in the AT of the PLWH were significantly and quantitatively higher.

We previously established that Vpr mice develop a striking fatty liver phenotype, driven by upregulation of the enzymatic machinery that regulates de novo lipogenesis in the liver (12). Upregulated hepatic lipogenesis in the face of excessive adipocyte lipolysis and inadequate AT energy sequestration is a common feature of many forms of lipodystrophy, including HIV-associated lipodystrophy (48,49). We have demonstrated that Vpr promiscuously activates transcription factors that regulate lipolysis and lipogenesis in the periphery (12,13). The present data support the concept that Vpr expression might stimulate ATF2 and the CREB axis to permit constitutive UCP1 expression in the face of persistent adrenergic stress (50). Our results reinforce the model that Vpr exerts multiple impacts on transcription factor networks that ultimately couple maladaptive AT function to fatty liver, dyslipidemia, and diabetes in PLWH.

Acknowledgments. The authors thank the BCM Advanced Technology Cores for use of the following facilities: Gene Vector Core (where hUCP1 reporter plasmids were generated by Ashkaan Moinzadeh and Kazuhiro Oka), Pathology and Histology Core, and Mouse Metabolism and Phenotyping Core. The authors thank the participants for volunteering for the study.

Funding. This work was funded by the Rutherford Diabetes Research Fund (to A.B.), and American Diabetes Association grant #1-18-IBS-105 and R01DK114356 (to S.M.H.). The study was also funded in part by an award from the BCM Nutrition and Obesity Pilot and Feasibility Fund and the Nancy Chang, PhD Award for Research Excellence. The adipose tissue samples from PLWH were obtained from New Works Concept Sheet 492 of the AIDS Clinical Trials Group. The study was supported by the National Institutes of Health National Institute of Allergy and Infectious Diseases grants UM1 AI068634, UM1 AI68636, UM1 AI106701, and K23 AI110532 (to J.E.L.). The work was also supported by National Institutes of Health, National Institute of Diabetes and Digestive and Kidney Diseases grant R01DK126042 (to J.E.L.).

The content of this publication is solely the responsibility of the authors and does not necessarily represent the official views and policies of the National Institutes of Health or the Department of Health and Human Services, nor does mention of trade names, commercial products, or organizations imply endorsement by the U.S. Government.

Duality of Interest. No potential conflicts of interest relevant to this article were reported.

Author Contributions. N.A., D.I., P.S. and A.S. conducted experiments. N.A., S.M.H., and A.B. designed the research studies, analyzed data, and drafted the manuscript. A.R.C. and P.S. provided analytical support. Y.X., N.S.U., U.S., and J.E.L. provided reagents and acquired data. All authors reviewed and edited the manuscript. A.B. is the guarantor of this work, and such had full access to all the data in the study and takes responsibility for the integrity of the data and the accuracy of the data analysis.

Prior Presentation. This work was presented in abstract form at the 80th Scientific Sessions of the American Diabetes Association, 12–16 June 2020.

References

1. Carr A, Miller J, Law M, Cooper DA. A syndrome of lipoatrophy, lactic acidaemia and liver dysfunction associated with HIV nucleoside analogue therapy: contribution to protease inhibitor-related lipodystrophy syndrome. AIDS 2000;14:F25–F32

2. Lyons MJ, Faust IM, Hemmes RB, Buskirk DR, Hirsch J, Zabriskie JB. A virally induced obesity syndrome in mice. Science 1982;216:82–85

3. Ramesh S, Sanyal AJ. Hepatitis C and nonalcoholic fatty liver disease. Semin Liver Dis 2004;24:399–413

4. Dhurandhar NV. A framework for identification of infections that contribute to human obesity. Lancet Infect Dis 2011;11:963–969

5. Torriani M, Fitch K, Stavrou E, et al. Deiodinase 2 expression is increased in dorsocervical fat of patients with HIV-associated lipohypertrophy syndrome. J Clin Endocrinol Metab 2012;97:E602–E607

6. Torriani M, Srinivasa S, Fitch KV, et al. Dysfunctional subcutaneous fat with reduced Dicer and brown adipose tissue gene expression in HIV-infected patients. J Clin Endocrinol Metab 2016;101:1225–1234

7. Srinivasa S, Wong K, Fitch KV, et al. Effects of lifestyle modification and metformin on irisin and FGF21 among HIV-infected subjects with the metabolic syndrome. Clin Endocrinol (Oxf) 2015;82:678–685

8. Srinivasa S, Torriani M, Fitch KV, et al. Brief report: adipogenic expression of brown fat genes in HIV and HIV-related parameters. J Acquir Immune Defic Syndr 2019;82:491–495

9. Cereijo R, Gallego-Escuredo JM, Moure R, et al. The molecular signature of HIV-1-associated lipomatosis reveals differential involvement of brown and beige/brite adipocyte cell lineages. PLoS One 2015;10:e0136571

10. Chouchani ET, Kajimura S. Metabolic adaptation and maladaptation in adipose tissue. Nat Metab 2019;1:189–200

11. Guallar JP, Gallego-Escuredo JM, Domingo JC, et al. Differential gene expression indicates that 'buffalo hump' is a distinct adipose tissue disturbance in HIV-1-associated lipodystrophy. AIDS 2008;22:575–584

12. Agarwal N, Iyer D, Gabbi C, et al. HIV-1 viral protein R (Vpr) induces fatty liver in mice via LXRα and PPARα dysregulation: implications for HIV-specific pathogenesis of NAFLD. Sci Rep 2017;7:13362

13. Agarwal N, Iyer D, Patel SG, et al. HIV-1 Vpr induces adipose dysfunction in vivo through reciprocal effects on PPAR/GR co-regulation. Sci Transl Med 2013;5:213ra164

14. Balasubramanyam A, Mersmann H, Jahoor F, et al. Effects of transgenic expression of HIV-1 Vpr on lipid and energy metabolism in mice. Am J Physiol Endocrinol Metab 2007;292:E40–E48

15. Henklein P, Bruns K, Sherman MP, et al. Functional and structural characterization of synthetic HIV-1 Vpr that transduces cells, localizes to the nucleus, and induces G2 cell cycle arrest. J Biol Chem 2000;275:32016–32026

16. Netanya S, Utay NS, Kitch DW, et al.; A5317 AIDS Clinical Trials Group Team. Telmisartan therapy does not improve lymph node or adipose tissue

fibrosis more than continued antiretroviral therapy alone. J Infect Dis 2018;217:1770–1781
17. Koh EH, Chernis N, Saha PK, et al. miR-30a remodels subcutaneous adipose tissue inflammation to improve insulin sensitivity in obesity. Diabetes 2018;67:2541–2553
18. Mina AI, LeClair RA, LeClair KB, Cohen DE, Lantier L, Banks AS. CalR: a web-based analysis tool for indirect calorimetry experiments. Cell Metab 2018;28:656–666.e1
19. Bachman ES, Dhillon H, Zhang CY, et al. betaAR signaling required for diet-induced thermogenesis and obesity resistance. Science 2002;297:843–845
20. Nosavanh L, Yu DH, Jaehnig EJ, Tong Q, Shen L, Chen MH. Cell-autonomous activation of Hedgehog signaling inhibits brown adipose tissue development. Proc Natl Acad Sci U S A 2015;112:5069–5074
21. Pluta K, Luce MJ, Bao L, Agha-Mohammadi S, Reiser J. Tight control of transgene expression by lentivirus vectors containing second-generation tetracycline-responsive promoters. J Gene Med 2005;7:803–817
22. Lizée G, Aerts JL, Gonzales MI, Chinnasamy N, Morgan RA, Topalian SL. Real-time quantitative reverse transcriptase-polymerase chain reaction as a method for determining lentiviral vector titers and measuring transgene expression. Hum Gene Ther 2003;14:497–507
23. Kharitonenkov A, Shiyanova TL, Koester A, et al. FGF-21 as a novel metabolic regulator. J Clin Invest 2005;115:1627–1635
24. Kharitonenkov A, Wroblewski VJ, Koester A, et al. The metabolic state of diabetic monkeys is regulated by fibroblast growth factor-21. Endocrinology 2007;148:774–781
25. Chau MD, Gao J, Yang Q, Wu Z, Gromada J. Fibroblast growth factor 21 regulates energy metabolism by activating the AMPK-SIRT1-PGC-1alpha pathway. Proc Natl Acad Sci U S A 2010;107:12553–12558
26. Harms M, Seale P. Brown and beige fat: development, function and therapeutic potential. Nat Med 2013;19:1252–1263
27. Cypess AM, Lehman S, Williams G, et al. Identification and importance of brown adipose tissue in adult humans. N Engl J Med 2009;360:1509–1517
28. Nedergaard J, Bengtsson T, Cannon B. Unexpected evidence for active brown adipose tissue in adult humans. Am J Physiol Endocrinol Metab 2007;293:E444–E452
29. Saito M, Okamatsu-Ogura Y, Matsushita M, et al. High incidence of metabolically active brown adipose tissue in healthy adult humans: effects of cold exposure and adiposity. Diabetes 2009;58:1526–1531
30. van Marken Lichtenbelt WD, Vanhommerig JW, Smulders NM, et al. Cold-activated brown adipose tissue in healthy men. N Engl J Med 2009;360:1500–1508
31. Virtanen KA, Lidell ME, Orava J, et al. Functional brown adipose tissue in healthy adults. N Engl J Med 2009;360:1518–1525
32. Couturier J, Agarwal N, Nehete PN, et al. Infectious SIV resides in adipose tissue and induces metabolic defects in chronically infected rhesus macaques. Retrovirology 2016;13:30
33. Couturier J, Lewis DE. HIV persistence in adipose tissue reservoirs. Curr HIV/AIDS Rep 2018;15:60–71
34. Couturier J, Suliburk JW, Brown JM, et al. Human adipose tissue as a reservoir for memory CD4+ T cells and HIV. AIDS 2015;29:667–674
35. Guilherme A, Yenilmez B, Bedard AH, et al. Control of adipocyte thermogenesis and lipogenesis through β3-adrenergic and thyroid hormone signal integration. Cell Rep 2020;31:107598
36. Johann K, Cremer AL, Fischer AW, et al. Thyroid-hormone-induced browning of white adipose tissue does not contribute to thermogenesis and glucose consumption. Cell Rep 2019;27:3385–3400.e3
37. Shabalina IG, Ost M, Petrovic N, Vrbacky M, Nedergaard J, Cannon B. Uncoupling protein-1 is not leaky. Biochim Biophys Acta 2010;1797:773–784
38. Rabhi N, Belkina AC, Desevin K, Cortez BN, Farmer SR. Shifts of immune cell populations differ in response to different effectors of beige remodeling of adipose tissue. iScience 2020;23:101765
39. Damouche A, Lazure T, Avettand-Fènoël V, et al. Adipose tissue is a neglected viral reservoir and an inflammatory site during chronic HIV and SIV infection. PLoS Pathog 2015;11:e1005153
40. Wanjalla CN, McDonnell WJ, Barnett L, et al. Adipose tissue in persons with HIV is enriched for $CD4^+$ T effector memory and T effector memory RA^+ Cells, which show higher CD69 expression and CD57, CX3CR1, GPR56 co-expression with increasing glucose intolerance. Front Immunol 2019;10:408
41. Deeks SG. HIV infection, inflammation, immunosenescence, and aging. Annu Rev Med 2011;62:141–155
42. Deeks SG, Tracy R, Douek DC. Systemic effects of inflammation on health during chronic HIV infection. Immunity 2013;39:633–645
43. Reilly SM, Saltiel AR. Adapting to obesity with adipose tissue inflammation. Nat Rev Endocrinol 2017;13:633–643
44. Couturier J, Winchester LC, Suliburk JW, et al. Adipocytes impair efficacy of antiretroviral therapy. Antiviral Res 2018;154:140–148
45. Kim SH, Chung JH, Song SW, Jung WS, Lee YA, Kim HN. Relationship between deep subcutaneous abdominal adipose tissue and metabolic syndrome: a case control study. Diabetol Metab Syndr 2016;8:10
46. Nookaew I, Svensson PA, Jacobson P, et al. Adipose tissue resting energy expenditure and expression of genes involved in mitochondrial function are higher in women than in men. J Clin Endocrinol Metab 2013;98:E370–E378
47. van den Beukel JC, Grefhorst A, Hoogduijn MJ, et al. Women have more potential to induce browning of perirenal adipose tissue than men. Obesity (Silver Spring) 2015;23:1671–1679
48. Sekhar RV, Jahoor F, White AC, et al. Metabolic basis of HIV-lipodystrophy syndrome. Am J Physiol Endocrinol Metab 2002;283:E332–E337
49. Hellerstein MK, Grunfeld C, Wu K, et al. Increased de novo hepatic lipogenesis in human immunodeficiency virus infection. J Clin Endocrinol Metab 1993;76:559–565
50. Cao W, Daniel KW, Robidoux J, et al. p38 mitogen-activated protein kinase is the central regulator of cyclic AMP-dependent transcription of the brown fat uncoupling protein 1 gene. Mol Cell Biol 2004;24:3057–3067